QUANTIFYING BONE DENSITY USING CONVENTIONAL RADIOGRAPHY

Kristin Rominger (Edward Hsu, PhD)
Department of Biomedical Engineering

Introduction

Osteoporosis is a major cause of morbidity and mortality worldwide. It is responsible for more than 8.9 million fractures annually [1], affecting 1 in 3 women and 1 in 5 men over the age of 50 [2], [3]. Since osteoporosis cannot be reversed, early diagnosis is critical in preventing and reducing the debilitating effects of a loss of bone density [4].

The gold standard for diagnosing osteoporosis is dual-energy x-ray absorptiometry (DXA) [4]. This technique uses two x-ray beams of different energies to differentiate soft tissue densities from bone mineral density (BMD). DXA-obtained BMD measurements of the femur, hip, and lumbar vertebrae are most commonly used to estimate bone fracture risk and diagnose osteoporosis [4], [5]. However, whole-body DXA scanners are expensive and only available in large cities and healthcare centers [6], [7]. Although portable BMD devices are available, they remain costly and are confined to use for peripheral measurements. Since these devices do not measure BMD of the femur, hip, or lumbar vertebrae, they are unsuitable for diagnostic use. Quantitative ultrasound is one portable BMD technique that attempts to lower costs, but is still under development and currently used as a pre-screening tool to identify candidates for DXA scanning [8].

An imaging modality that is relatively low-cost and widespread throughout both developed and developing countries is conventional radiography [5]. When radiographic scanners were equipped with an intensity calibration device during imaging, the intensities in the radiograph were successfully related to standardized mass quantities, a necessity for quantifying BMD [6].

Due to these reasons, conventional radiography offers an alternative to costly and inaccessible DXA scanners. Although there exists a motivation to quantify bone density from radiographic images, methods to do so are currently undeveloped. To make radiographs suitable for quantitative BMD measurements, the soft tissues of the anatomy need to be separated from the bone, and the thickness of the bone needs to be accounted for.

In this study, we developed a preliminary method to quantify bone density using radiographs. We employed geometrical modeling of both the cortical bone and the soft tissues of a radiograph dataset to account for bone thickness and estimate bone density without interference from soft tissues. For validation, we compared bone densities obtained using our method to CT density measurements of the same subjects. We also compared the CT density measurements to baseline radiograph densities that were obtained without modeling. To quantify our results and determine correlation between CT density measurements and the baseline and modeled densities obtained from the radiographs, we performed linear regression analysis. This work constitutes progress towards a low-cost, widely accessible method for diagnosing osteoporosis that is especially needed in developing countries.

Methods

Radiograph Dataset Selection and Backgrounding

　　To quantify bone mineral density from radiographs, we applied a second-order soft tissue model to estimate tibial and metacarpal bone mineral densities from the radiographs of 15 parrots (8 Sun Conures, 7 Quakers). The parrots were imaged with an intensity calibration device consisting of six plastic washers whose masses varied linearly. We first subtracted the background intensity of each image from the full image, setting the background intensities to zero, before constructing a calibration curve that related intensities of the standardized intensity calibration device to their mass quantities. Backgrounding, construction of the calibration curve, and all further manipulation and modeling of the radiographs were performed in MATLAB R2016b (MathWorks, Natick MA).

Region of Interest Selection with Noise Reduction

　　The midline of the bottom tibia in each image was fit to a linear equation to align the image coordinates with the axis of the tibia (Fig. 1A) and calculate the indices ranging between 20% and 50% of tibial length (measured with respect to the distal end). This region of the tibia closely approximated a cylindrical shape and was used for modeling. With the axis of the tibia aligned with image coordinates, the intensity values were recorded by horizontal position. We averaged the intensity of each horizontal position in sets of ten vertically adjacent pixels. This averaging was performed to reduce the effects of noise in order to generate more representative intensity profiles and facilitate modeling.

Soft Tissue Modeling

From the plotted intensity profiles of each set of measurements (Fig. 1B), the intensities of the soft tissues were modeled as quadratic functions and digitally subtracted from the original scan of the tibia to create a 'bone only' scan (Fig. 1C). The intensities located in the coordinates containing the tibia bone itself were neglected during the modeling of the quadratic function, but the subtraction was applied to all intensities.

Bone Density Quantification

　　The bone density of each parrot was quantified from its bone only scan by modeling each tibia as a concentric cylinder with a hollow interior. The two peak intensities observed in each bone only intensity profile (Fig. 1D) correspond to the projection of the intensities of the cortical bone. These values were averaged and divided by the number of pixels that the intensity sum was calculated over, generating a relative density value for each parrot. Eq. 1, derived directly from the Pythagorean Theorem, shows the calculation for the total number of pixels that each intensity was calculated over (n), where r_{out} is the outer diameter of the cortical bone and r_{in} is the inner diameter of the cortical bone.

$$n = 2\sqrt{{r_{out}}^2 - r_{in}^2} \quad \text{(Eq. 1)}$$

Each relative density value was converted to a standardized density value using the constructed calibration curve.
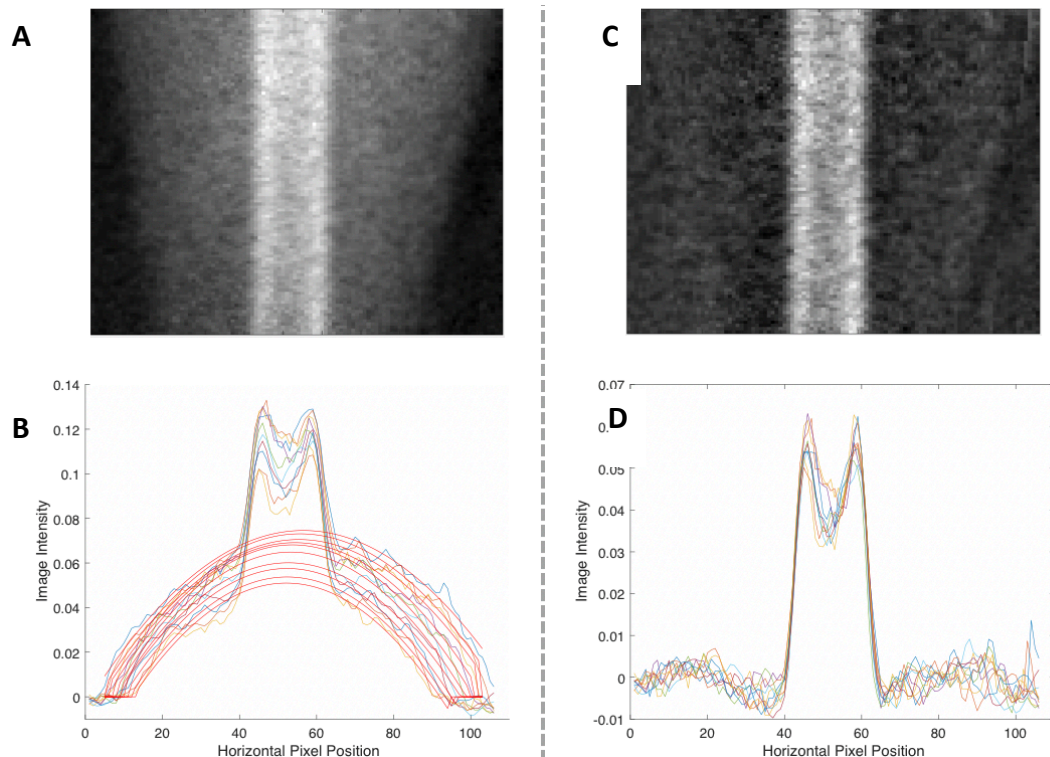
Fig. 1: Intensity profiles of original and bone-only radiograph images of the tibia. The original image (**A**) is shown directly above its intensity profile along the length of the tibia (**B**), with soft tissues modeled in red. Note that each intensity profile curve corresponds to the averaged intensities of 10 vertically adjacent pixels for a given horizontal pixel location. The bone-only image (**C**) is the original image with the modeled soft tissue intensities removed. Its intensity profile is shown directly below (**D**).

Validation and Statistical Analysis

To serve as a baseline for comparison, 'uncorrected' density calculations from the same radiograph scans were obtained without performing any geometrical modeling or soft tissue removal. These calculations were performed on the same tibias, in the same locations (between 20% and 50% of tibia length measured with respect to the distal end). They followed the same procedures as the corrected radiograph intensities for density quantification, with the exception that the intensities used for density quantification were taken from the original image with soft tissue intensities included, and without accounting for the number of pixels that the intensities were taken over.

Both the uncorrected and corrected radiograph densities were compared to CT measurements, which represent the accepted densities. CT scans of the same 15 parrot dataset were obtained. Since the CT scans featured the birds in different positions than the radiograph scans (and thus could not be correlated to the correct tibia used for the radiograph analysis), CT density measurements of both tibias were taken and averaged. These CT measurements were taken using Amira (Thermo Scientific, Waltham MS), 3D software used for CT visualization and analysis. These measurements were in Hounsfield units (HU), which are linear in scale, and were taken and averaged over the same locations as in the radiographs (between 20% and 50% of tibia length measured with respect to the distal end) by selecting this region.

Both the uncorrected and corrected radiograph measurements were independently compared to the CT measurements. We performed linear regression analysis of uncorrected radiograph measurements vs. CT measurements and corrected radiograph measurements vs. CT

measurements to determine R^2 values for each relation, and whether a significant correlation could be established for each relation. R^2 values vary from 0 to 1 and represent the percent of variation in the radiograph model that is predicted by the CT measurements, with values closest to 1 representing the best fit between the radiograph predictions and the CT measurements. In addition, hypothesis testing of the slope of each regression line was performed using a t-test (with associated p-values) to test the null hypothesis that the slope is not statistically different than zero, using a minimum confidence level of 95%. A slope of zero implies that there is no significant linear relationship between the radiograph and CT densities, as a change in CT density would not be reflected by a change in radiograph density. A low p-value ($p < 0.05$) suggests that the slope is not zero, and that changes in CT density are associated with changes in radiograph density. This is necessary for radiograph densities to be representative of CT densities. Finally, the entire process of bone density quantification, validation, and statistical analysis was repeated for the leftmost metacarpal in each parrot radiograph of the dataset.

Results

The uncorrected and corrected tibial densities, plotted against the corresponding CT densities for each parrot, are shown in Figures 2 and 3, respectively. For the uncorrected radiograph densities, a positive slope was found at the 95% confidence level ($p = 0.04$) from the regression analysis, with an R^2 of 0.29 for the regression equation. From this equation, uncorrected tibial radiograph density is predicted to equal $2.00 + 0.0032 \cdot (CT\ density)$, when *CT density* is reported in HU and radiograph density is reported in standardized intensity calibration device units. When modeling was applied to the radiographs, a positive slope was found at a higher confidence level of 99.995% ($p = 0.0001$) from the regression analysis, and R^2 improved to 0.70 for the regression equation. From this equation, tibial radiograph density is predicted to equal $2.32 + 0.0069 \cdot (CT\ density)$, when *CT density* is reported in HU and radiograph density is reported in terms of standardized intensity calibration device units.
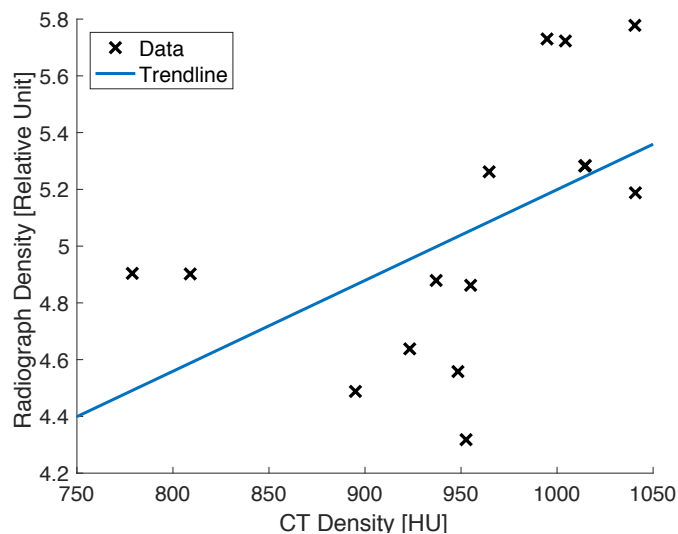
Fig. 2: Uncorrected radiograph densities compared to CT densities in the tibias of 15 parrots. Linear trendline: $y = 0.0032x + 2.00$ ($p < 0.05$, $R^2 = 0.29$). Note that radiograph density units are reported in terms of the standardized intensity calibration device, which is linear in scale.
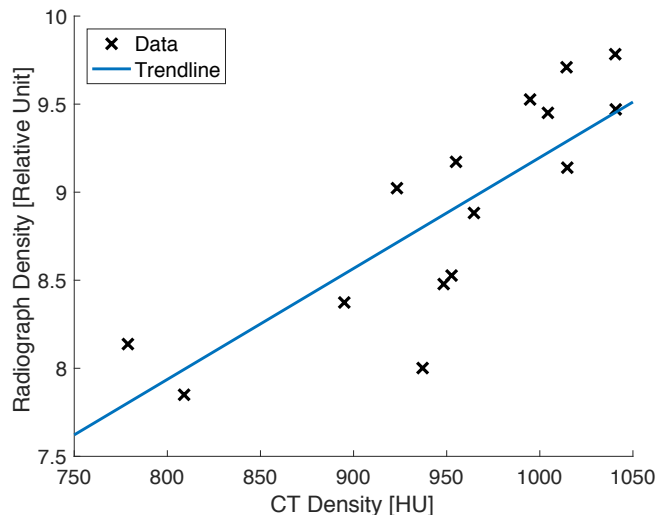
Fig. 3: Corrected radiograph densities compared to CT densities in the tibias of the 15 parrots. Linear trendline: $y = 0.0069x + 2.32$ (p < 0.0005, $R^2 = 0.70$).

Figures 4 and 5 show the uncorrected and corrected metacarpal densities, respectively, plotted against the corresponding CT densities for each parrot. Results from simple linear regression indicate that a non-zero slope could not be found at a 95% confidence level for either the uncorrected or corrected radiograph densities. For the uncorrected radiograph densities, simple regression analysis resulted in a p-value of 0.3, with an R^2 of 0.080. From this analysis, uncorrected metacarpal radiograph density is predicted to equal $0.21 + 0.00023 \cdot (CT\ density)$, when *CT density* is reported in HU and radiograph density is reported in standardized intensity calibration device units. When modeling was applied to the radiographs, simple regression analysis resulted in a p-value of 0.2, and R^2 improved slightly to 0.14. Based on this analysis, metacarpal radiograph density is predicted to equal $7.79 + 0.0054 \cdot (CT\ density)$, when *CT density* is reported in HU and radiograph density is reported in terms of standardized intensity calibration device units.
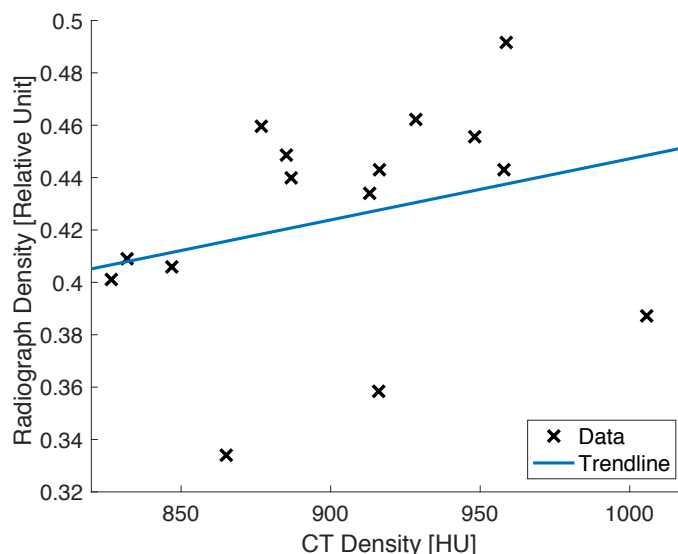
Fig. 4: Uncorrected radiograph densities compared to CT densities in the metacarpals of 15 parrots. Linear trendline: $y = 0.00023x + 0.21$ (NS, $R^2 = 0.080$).
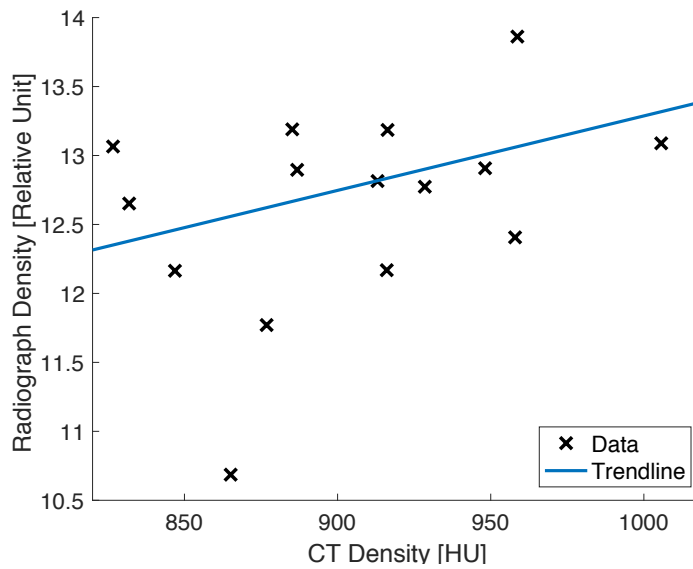
Fig. 5: Corrected radiograph densities compared to CT densities in the metacarpals of the 15 parrots. Linear trendline: $y = 0.0054x + 7.79$ (NS, $R^2 = 0.14$).

Discussion

This study is a first attempt to quantify bone density using soft-tissue modeling of radiographs. We used intensity calibration and second-order modeling of soft tissues to determine the bone densities of radiographs at the tibial and metacarpal sites. Based on the comparison of these results to CT-obtained bone densities of each site, a significant correlation between the densities from the radiographs and those from CT was found for the tibial site, but not the metacarpal site.

A significant correlation between the bone density derived from the modeled radiographs and the CT measurements (accepted densities) was found at the tibial site ($R^2 = 0.70$, $p < 0.0005$) (Fig. 3). Based on this relatively high R^2 value, the tibial densities obtained from the modeled radiographs are generally representative of the accepted density values. This result also marked a significant improvement from the baseline (unmodeled) radiograph densities, which featured a weaker correlation ($R^2 = 0.29$, $p < 0.05$) (Fig. 2). The difference in the two results is due solely to soft-tissue modeling, demonstrating its significance in determining the bone density of radiographs at the tibia.

However, a significant correlation between the modeled radiograph and CT densities was not found for the metacarpal site ($R^2 = 0.14$, NS) (Fig. 5). Although there was a slight increase in R^2 when comparing this result to the baseline correlation ($R^2 = 0.080$, NS) (Fig. 4), the correlation remained non-significant and the modeled radiograph densities were not representative of the CT densities at the metacarpal site. The difference in the significance in correlation between the tibial and metacarpal sites is likely due to the differences in geometry and surrounding skeletal structure of the two sites. The tibial site is relatively isolated from surrounding bones and is also geometrically simple in shape, closely approximating a concentric cylinder. In contrast, the metacarpal site features overlapping bones and feathers and has irregular geometry that our model may have had trouble accounting for.

When comparing the tibial site results from our radiograph-based method to results obtained from other portable or peripheral BMD quantification devices, the tibial site featured

strong correlation to accepted BMD [10]-[13]. These other quantification devices are most likely to be used in areas without access to standard equipment, such as DXA scanners, and serve as a standard-for-comparison for our radiograph-based technique. In one study, Kim et al. tested the association of speed of sound measured by ultrasound densitometry with bone mineral density measured by DXA in seven sites throughout the spine, femur, and forearm. They found r values ranging from 0.63 to 0.78 (all $p < 0.0001$), corresponding to R^2 values ranging from 0.40 to 0.61 [10].

Similarly, Kayalar et al. tested the association of BMD measurements of the calcaneus (heel bone) obtained from the DXA Laser Calscan device with T-scores obtained from traditional DXA. T-scores are calculated from the measured BMD value, representing the number of standard deviations that the BMD value varies from the average BMD of a 25-year-old of the same sex. The Calscan device is more mobile and less costly when compared to traditional DXA, but features relatively low correlation when compared to results from traditional DXA scanners, with $r = 0.340$ ($p = 0.001$), corresponding to $R^2 = 0.12$ [11].

Finally, portable DXA scanners that measure the bone density of peripheral sites including the forearm and fingers have been compared to traditional DXA measurements of the hip and spine. Comparison of the BMD measurements from AccuDXA 2 portable scanner with those from traditional DXA resulted in $r = 0.61$ ($p < 0.001$) for women, corresponding to $R^2 = 0.37$, and $r = 0.53$ ($p < 0.001$) for men, corresponding to $R^2 = 0.28$ [12]. When compared with T-scores of the hip using traditional DXA, T-scores of the forearm from the Osteometer-DTX200 peripheral DXA scanner resulted in $r = 0.34$ ($p < 0.05$), corresponding to $R^2 = 0.12$ [13].

Although all of the correlations presented from these portable or peripheral BMD quantification devices were statistically significant, the correlations were often relatively weak. The R^2 value obtained using BMD measurements of the tibial site after soft-tissue modeling was performed surpassed that of the other techniques presented, indicating its potential utility. However, there are limitations with this study that may affect the comparison of its results with the other methods. Most significantly, we applied our analysis to a parrot dataset rather than a human dataset and used CT, rather than DXA, to validate. Differences in the trabecular and cortical bone content between humans and parrots may yield different success in quantifying BMD in humans with the radiograph-based method. In addition, the BMD measured in the parrots consisted almost entirely of cortical bone, while osteoporosis in humans primarily causes a decrease in the BMD of trabecular bone. Using CT to validate our method also limits the utility of our results, as the radiograph-derived BMD results would ideally be put into the context of DXA-obtained measurements since current diagnostic criteria for osteoporosis have been developed from DXA. Finally, by quantifying BMD from a single tibia from each radiograph, this study assumed that both the left and right tibia had approximately the same bone density, which may introduce small inaccuracies into our results.

Despite these limitations, this study was able to demonstrate that intensity calibration and soft-tissue modeling of radiographs can yield representative bone density measurements for an isolated, geometrically simple site (tibia) in a research context. This study also demonstrates the significance of soft-tissue modeling in accurately determining the relative intensity of embedded structures. This may have applications in areas such as oncology, as it could potentially be used to enhance bone tumor visualization using conventional radiography. In addition, by demonstrating that a technique based on conventional radiography can be used to quantify bone density, this study offers a potential method to diagnose osteoporosis in developing countries where DXA and CT are largely inaccessible. An "add-on" system consisting of the intensity calibration device and the software capable of quantifying bone density using soft-tissue

modeling could be eventually be supplied to facilities that own a conventional x-ray scanner, which are much more widespread than either CT or DXA scanners.

Before this radiograph-based system can be adapted clinically, there are several key developments that first need to occur. Future work includes applying the system to a human dataset and validating its results with DXA-obtained bone densities. In addition, the technique needs to be automated (*e.g.*, user-selection of soft tissue boundaries needs to be removed) and converted into a programming language that is compatible with conventional x-ray scanners. Finally, algorithms need to be developed to better detect and account for overlap when quantifying bone. Successfully introducing these developments would result in a low-cost, widely accessible method to diagnose osteoporosis in developing countries where osteoporosis often goes undiagnosed, resulting in debilitating bone fractures that may be preventable with earlier diagnosis and preventative measures.

Conclusion

In this study, we developed a preliminary method to quantify bone density using radiographs, employing geometrical modeling of both cortical bone and soft tissues of a radiograph dataset to estimate bone density without interference from soft tissues. We were able to successfully quantify bone densities in the tibia, as validated by CT measurements. Greater correlation to absolute density was observed for our method as compared to other peripheral or low-cost methods that aim to be used in developing countries or other areas where DXA scanners are not available. However, future work needs to be done to address sites with greater overlap or more irregular geometry before this method can be employed clinically. Ultimately, this work constitutes progress towards a low-cost, widely accessible method for osteoporosis diagnosis in developing countries.

References

[1] O. Johnell and J. A. Kanis, "An estimate of the worldwide prevalence and disability associated with osteoporotic fractures," *Osteoporos. Int.*, vol. 17, no. 12, pp. 1726– 1773, 2006.

[2] L. J. Melton, E. A. Chrischilles, C. Cooper, A. W. Lane, and B. L. Riggs, "Perspective. How many women have osteoporosis?" *J. Bone Miner. Res.*, vol. 20, no. 5, pp. 826– 892, 1992.

[3] L. J. Melton, E. J Atkinson, M. K. O'Connor, W. M. O'Fallon, and B. L. Riggs, "Bone density and fracture risk in men," *J. Bone Miner. Res.*, vol. 13, no. 12, pp. 1915– 1923, 1998.

[4] J. M. Kling, B. L. Clarke, and N. P. Sandhu, "Osteoporosis prevention, screening, and treatment: a review," *J. Womens Health*, vol. 23, no. 7, pp. 563– 572, 2014.

[5] M. K. Garg and S. Kharb, "Dual energy x-ray absorptiometry: pitfalls in measurement and interpretation of bone mineral density," *Indian J. Endocrinol. Metab.*, vol. 17, no. 2, pp. 203 – 210, 2013.

[6] International Osteoporosis Foundation, "The Asian Audit: Epidemiology, costs and burden of osteoporosis in Asia 2009," *International Osteoporosis Foundation*, 2009. Available: https://www.iofbonehealth.org/sites/default/files/PDFs/Audit%20Asia/Asian_regional_audit_2009.pdf. [Accessed Nov. 2, 2017].

[7] R. Handa, A. Ali Kalla, and G. Maalouf, "Osteoporosis in developing countries," *Best Prac. Res. Clin. Rheumat.*, vol. 22, no. 4, pp. 693– 708, 2008.

[8] K. Thomsen, D. Jepsen, L. Matzen, A. Hermann, T. Masud, and J. Ryg, "Is calcaneal quantitative ultrasound useful as a prescreen stratification tool for osteoporosis?" *Osteoporos. Int.*, vol. 26, no. 5, pp. 1459– 1475, 2015.

[9] M. S. Echols and E. W. Hsu, "Validation of a novel radiograph density determination process: a multicenter study," *in 37th Ann. Conf. and Expo. of Assoc. Avian Vet. (AAV),* Portland, USA, Aug. 27-Sept. 1, 2016, pp. 39.

[10] K. I. Kim, I. K. Han, H. Kim, and N. H. Cho, "How reliable is the ultrasound densitometer for community screening to diagnose osteoporosis in the spine, femur, and forearm?" *J. Clin. Densitom*, vol. 4 no. 2, pp. 159– 165, 2001.

[11] G. Kayalar, A. Cevikol, G. Yavuzer, Y. Sanisoglu, A. Cakci, and T. Arasil, "The value of calcaneal bone mass measurement using a dual x-ray laser calcscan device in risk screening for osteoporosis," *Clinics (Sao Paolo)*, vol. 64, no. 8, pp. 757– 762, 2009.

[12] D. von Muhlen, D. Claflin, and E. Barrett-Connor, "A cross-sectional association of phalangeal bone mineral density versus hip bone mineral density with osteoporosis and non-vertebral fracture," *J. Clin. Densitom*, vol. 12, no. 3, pp. 392– 392, 2009.

[13] V. K. Wadhwa and N. J. Parr, "Peripheral or axial bone density measurements to identify osteoporosis in prostate cancer patients undergoing androgen deprivation therapy," *Urology*, vol. 73, no. 6, pp. 1347– 1351, 2009.